Asian Journal of Pharmaceutical Sciences 15 (2020) 646–660

Available online at www.sciencedirect.com

ScienceDirect

journal homepage: www.elsevier.com/locate/AJPS

Original Research Paper

Enhanced anticancer effect of doxorubicin by TPGS-coated liposomes with Bcl-2 siRNA-corona for dual suppression of drug resistance

Yinghuan Li[a], *Xi Tan*[b], *Xuhan Liu*[b], *Lingyan Liu*[a], *Yan Fang*[b], *Rong Rao*[b], *Yuanyuan Ren*[b], *Xiangliang Yang*[b,c], *Wei Liu*[b,c,*]

[a] *School of Pharmaceutical Sciences, Beijing Area Major Laboratory of Peptide and Small Molecular Drugs, Engineering Research Center of Endogenous Prophylactic of Ministry of Education of China, Capital Medical University, Beijing 100069, China*

[b] *College of Life Science and Technology, Huazhong University of Science and Technology, Wuhan 430074, China*

[c] *National Engineering Research Center for Nanomedicine, Huazhong University of Science and Technology, Wuhan 430074, China*

ARTICLE INFO

Article history:
Received 14 January 2019
Revised 30 July 2019
Accepted 9 October 2019
Available online 12 November 2019

Keywords:
Multiple drug resistance (MDR)
TPGS
siRNA-corona
Liposomes
P-glycoprotein (P-gp)
Bcl-2

ABSTRACT

Multiple drug resistance (MDR) is a tough problem in developing hepatocellular carcinoma (HCC) therapy. Here, we developed TPGS-coated cationic liposomes with Bcl-2 siRNA corona to load doxorubicin (Dox) *i.e.*, Bcl-2 siRNA/Dox-TPGS-LPs, to enhance anticancer effect of Dox in HCC-MDR. TPGS *i.e.*, D-α-tocopheryl polyethylene glycol 1000 succinate, inhibited P-glycoprotein (P-gp) efflux pump and Bcl-2 siRNA suppressed anti-apoptotic Bcl-2 protein. The Bcl-2 siRNA loaded in the liposomal corona was observed under transmission electron microscopy. The stability and hemolysis evaluation demonstrated Bcl-2 siRNA/Dox-TPGS-LPs had good biocompatibility and siRNA-corona could protect the liposomal core to avoid the attachment of fetal bovine serum. In drug-resistant cells, TPGS effectively prolonged intracellular Dox retention time and siRNA-corona did improve the internalization of Dox from liposomes. *In vitro* and *in vivo* anticancer effect of this dual-functional nanostructure was examined in HCC-MDR Bel7402/5-FU tumor model. MTT assay confirmed the IC_{50} value of Dox was 20–50 fold higher in Bel7402/5-FU MDR cells than that in sensitive Bel7402 cells. Bcl-2 siRNA corona successfully entered the cytosol of Bel7402/5-FU MDR cells to downregulate Bcl-2 protein levels *in vitro* and *in vivo*. Bcl-2 siRNA/Dox-TPGS-LPs showed superior to TPGS- (or siRNA-) linked Dox liposomes in cell apoptosis and cytotoxicity assay in Bel7402/5-FU MDR cells, and 7-fold greater effect than free Dox in tumor growth inhibition of Bel7402/5-FU xenograft nude mice. In conclusion, TPGS-coated cationic liposomes with Bcl-2 siRNA corona had the capacity to inhibit MDR dual-pathways and subsequently improved the anti-tumor activity of the chemotherapeutic agent co-delivered to a level that cannot be achieved by inhibiting a MDR single way.

* Corresponding author. College of Life Science and Technology, Huazhong University of Science and Technology, Luoyu Road 1037, Wuhan 430074, China. Tel.: +86 27 87792147
E-mail address: wliu@hust.edu.cn (W. Liu).
Peer review under responsibility of Shenyang Pharmaceutical University.

https://doi.org/10.1016/j.ajps.2019.10.003

1. Introduction

The occurrence of multiple drug resistance (MDR) is generally associated with cancer treatment failure of chemotherapy [1]. MDR is frequently caused by long-term exposure to cytotoxic drugs or intrinsic in some tumor cells [2]. There have been various reports of MDR mechanisms, including enhanced efflux or reduced uptake of chemotherapeutic agents, activation of cellular anti-apoptotic defense proteins or inactivation of apoptosis pathways, recovery of DNA repair, and detoxification [3–6]. Vitamin E TPGS, *i.e.*,D-α-tocopheryl polyethylene glycol 1000 succinate, was used to modify nanoparticles by inhibiting a single mechanistic pathway to overcome P-glycoprotein (P-gp) efflux [7]. However, the overall MDR phenotype in a tumor could be resulted from a combination of effects by various underlying mechanisms and consequently to inhibit a single mechanistic pathway is often not sufficient to overcome MDR [8–10].

We hypothesize that suppressing efflux pump such as P-gp and anti-apoptotic protein such as Bcl-2 simultaneously could improve anticancer effect through dual MDR reversal. To test our hypothesis, we first developed TPGS-coated liposomes with Bcl-2 siRNA-corona for simultaneous suppression of P-gp and Bcl-2 and then tested whether this novel nanostructure would enhance the efficacy of co-delivered chemotherapeutic agent doxorubicin (Dox) in hepatocellular carcinoma (HCC) Bel7402/5-FU MDR model.

P-gp is an adenosine triphosphate (ATP) consuming membrane-bound pump that effuses and decreases intracellular concentration of various chemotherapeutic agents including Dox [11]. Co-administration of verapamil (a small molecule P-gp inhibitor) has demonstrated increased efficacy of anti-tumor medicines in chemoresistant malignancies, accompanying with potential side effects related to its dose [12,13]. TPGS, a P-gp ATPase inhibitor approved by FDA, has been used as an adjuvant treatment [14]. Structurally, TPGS is a nonionic amphiphilic polymer containing hydrophilic polyethylene glycol (PEG) 1000 and hydrophobic α-tocopherol succinate (Vitamin E derivative) [15]. The PEG fragment in TPGS increases the stability of cationic liposomes and extends the systemic circulation half-life. In literature, TPGS inhibits P-gp efflux and helps achieve higher intracellular Dox concentration.

The expression of cellular anti-apoptotic Bcl-2 protein represents another different molecular mechanism causing MDR. Evidence showed that upregulated and downrgulated Bcl-2 protein weakened chemotherapy-induced apoptosis and improved cancer treatment outcomes, respectively [16,17]. The Bcl-2 protein expression was down-regulated by Bcl-2 siRNA with a sequence-specific manner. Due to electrostatic interactions, Bcl-2 siRNA was attached to the cationic liposomes surface. Thus, the siRNA-corona was observed on the surface of cationic Dox liposomes. Transmission electron microscopy (TEM) images have confirmed the siRNA-corona structure in the outer layer or surface of liposomes. In the current study we tested whether the siRNA-corona would maintain siRNA transfection functionality to downregulate anti-apoptotic Bcl-2 protein.

HCC is one kind of cancer with high incidence and mortality, with the problem of drug resistance continuing to increase every year [18–20]. HCC Bel7402/5-FU MDR model was established since it increased over 5-fold resistance to Dox compared to parental Bel7402 cells [21,22]. The IC_{50} value of Dox measured by MTT assay was 20–50 times higher in Bel74025/5-FU MDR cells than the non-MDR cells. Bel7402/5-FU cells were selected as common MDR models to study Dox resistance in various experiments [23,24].

Dox was selected as a model chemotherapeutic agent for its well-known broad-spectrum anticancer activity and the currently available methodologies in preparation of Dox-loaded liposomes [25]. Cationic liposomes have been widely adopted as siRNA carriers to improve transfection. The detailed lipids composition for the cationic liposomes in our current study is described in the method. The key formulation design rationale and the proposed functionality of each component in the formulation are shown in Fig. 1. In brief, TPGS-linked liposomes with Bcl-2 siRNA-corona inhibited P-gp efflux, promoted Dox internalization, down-regulated Bcl-2 protein level, enhanced cell apoptosis and cytotoxicity, increased *in vivo* anti-tumor efficacy.

2. Material and methods

2.1. Materials

D-α-Tocopherol polyethylene glycol 1000 succinate (TPGS) was obtained from Sigma-Aldrich (Shanghai, China). 1,2-distearoyl-sn–glycero-3-phosphoethanolamine-N-[methoxy (polyethylene glycol)−2000] (PEG-DSPE), 1,2-dioleoyl-3-trimethylammoniumpropane (DOTAP), and 1,2-dipalmitoylsn–glycero-3-phosphocholine (DPPC) were obtained from Avanti Polar Lipids, Inc. (Alabaster, USA). Cholesterol (CH) was from Sinopharm Chemical Reagent Co., Ltd. (Shanghai, China). Doxorubicin hydrochloride (Dox) was purchased from Meso Chemical Technology Co., Ltd. (Beijing, China). 3-(4,5-dimethylthiazol-2-yl)−2,5-diphenyl tetrazolium bromide (MTT) and 4′,6-Diamidino-2-phenylindole (DAPI) were from Biosharp Co., Ltd. (Hefei, China). Paraformaldehyde solution (4%) was obtained from Solarbio Life Science Co., Ltd. (Beijing, China). Ammonium sulfate and dimethyl sulfide (DMSO) were from Sinopharm Chemical Reagent Co., Ltd. (Shanghai, China). All other reagents and solvents were of either analytical or HPLC grade. Targeting human Bcl-2 siRNA (sence: 5′UUAUCCUGGAUCCAGGUGUGGAGGU −3; antisence: 5′ACGCUGGGAGAACAGGGUACGAUAA-3′) and FAM-labeled scrambled siRNA (FAM-siRNA) were purchased from Invitrogen (USA). Propidium Iodide (PI) and Annexin-V-FITC Apoptosis Kit were obtained from Beyotime Biotechnology (Shanghai, China). The FITC-mouse anti-human P-glycoprotein (P-gp antibody, material number 557002) and IgG2b κ isotype control (isotype antibody serving as control groups, material number 555742) were purchased from Becton Dickinson (CA, USA).

2.2. Formulation difference of various Dox-loaded liposomes

Thin-film hydration method followed by ammonium sulfate gradient loading procedure was used to prepare Dox-loaded

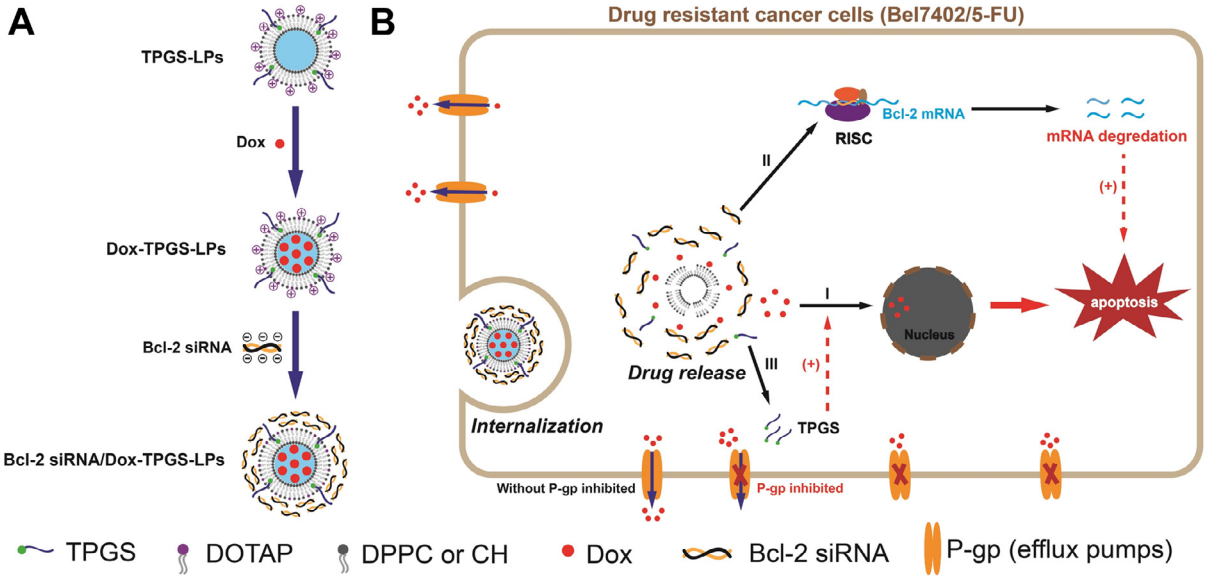

Fig. 1 – Schematic representation of TPGS-coated cationic liposomes with Bcl-2 siRNA-corona to load doxorubicin (Dox). (A) The preparation process and the structure of Bcl-2 siRNA/Dox-TPGS-LPs. (B) Overcoming MDR by combined inhibition of P-gp pump and Bcl-2 protein with Bcl-2 siRNA/Dox-TPGS-LPs. I: Dox release in cytosol and uptake in nuclei; II: Released Bcl-2 siRNA in cytosol to trigger RNA-induced silencing complex (RISC) for eliminating Bcl-2 mRNA to down-regulate the expression of Bcl-2 protein; III: Released TPGS to inhibit drug-efflux P-gp pump.

liposomes [26]. A chloroform solution of DOTAP, DPPC, CH and TPGS (or PEG-DSPE) at molar ratios of 40:40:16:4 was made and then evaporated to form a thin lipid film, which was further hydrated with 180 mM ammonium sulfate solution and extruded with a polycarbonate membrane at 100 nm pore size by a mini-extruder (Avanti Polar Lipids, Inc., USA) to prepare TPGS coated cationic liposomes or PEG-DSPE coated cationic liposomes. The external phase of blank liposomes was changed to 0.9% NaCl by diafiltration. Dox solution was added to empty liposomes (drug: lipid = 1:10, w/w), mixed for 30 min at 40 °C water bath to obtain Dox-loaded liposomes (Dox-PEG-LPs or Dox-TPGS-LPs). Dox-PEG-LPs were used as a control. The entrapment efficiency of Dox was measured by Sephadex G50 column and UV spectrophotometer (UV-1750, Shimadzu, Japan) at 482 nm.

In the next step, siRNA was electrostatically associated with cationic liposomes to obtain siRNA-loaded liposomes (*i.e.*, siRNA/Dox-TPGS-LPs or siRNA/Dox-PEG-LPs) [27]. Briefly, liposomes were diluted with DEPC water to the designed concentrations, transferred to siRNA solution with varing molar ratios of amino groups in cationic lipid (DOTAP) to phosphate groups in siRNA (*i.e.*, N/P ratios) and mixed through pipetting. The siRNA-loaded liposomes were continued incubation for 30 min at room temperature before characterization and gene silencing experiments. Entrapment efficiency of siRNA adsorption on the liposomal surface was determined by utra-centrifugation at 20 000 × g at 4 °C for 1 h [28].

The particle size and zeta potential of liposomes were measured by the dynamic light scattering method under a Malvern Zetasizer Nano machine (ZS90, Worcestershire, UK). The nanostructure of diluted liposomes was observed under TEM (H-7000FA, Hitachi, Japan) by laying liposomes stained with phosphotungstic acid on a carbon-coated copper grid. The stability of liposomes in PBS (pH 7.4) with or without 10% fetal bovine serum (FBS) was evaluated until 96 h.

The hemolysis test was conducted by adding various liposomes in normal saline containing 1% (v/v) mice erythrocytes at 37 °C for 1 h [29]. The total lipid concentration is 0.5 mg/ml (twice the dose for mice in Section 2.12). After centrifugation, the supernatant was collected and the released hemoglobin absorbance at 540 nm was measured. The blank saline was used as a negative control, while saline containing 1% Triton X-100 was used as the positive control for 100% hemolysis. The hemolysis ratio of liposome was calculated by the ratio between sample and Triton X-100.

2.3. *In vitro Dox release study*

Dox release from Dox-loaded liposomes and siRNA/Dox co-loaded liposomes *in vitro* were evaluated by dialysis method [30]. 1 ml of Dox-PEG-LPs, Dox-TPGS-LPs, Bcl-2 siRNA/Dox-PEG-LPs and Bcl-2 siRNA/Dox-TPGS-LPs were placed in the dialysis bag (MWCO 3500 Da) respectively. Liposomes-loaded dialysis bags were submerged in 100 ml of Tween 80 (1%, w/v)-containing PBS (0.01 M, pH 7.4) with shaking at 100 rpm. At predetermined time points, the external medium (1 ml) was collected and followed by addition of equal volum of fresh medium. Cumulative Dox release was measured at $\lambda_{Ex/Em}$ of 485/574 nm under fluorescence spectrophotometer (F-4500, Hitachi, Japan).

2.4. Cell culture and P-gp expression

Human hepatocellular carcinoma Bel7402 sensitive cells and Bel7402/5-FU MDR cells were purchased from Chinese Academy of Sciences (Shanghai, China) and cultured at 37 °C with 5% CO_2 in 95% humidity. Bel7402 cells culture was developed in DMEM medium (Hyclone®, UT, USA) containing 10% FBS and 1% streptomycin/penicillin (both from Gibco, CA, USA). Bel7402/5-FU cells culture was developed with full medium containing 20 μg/ml of 5-Fluororacil (5-FU, Sigma-Aldrich, Shanghai, China) to maintain the multidrug resistance. P-gp expression in both cells was measured by using antibody immunofluorescence standard protocols [11].

2.5. Intracellular Dox accumulation to evaluate the inhibitory effect on P-gp efflux

Quantitative analysis by flow cytometry was selected to calculate Dox accumulation in sensitive or MDR cells [31]. The Bel7402 or Bel7402/5-FU cells were seeded into 6-well plates and incubated for a day to reach the density of 8×10^5 cells per well. The cells were then treated with free Dox, Dox-PEG-LPs, Dox-TPGS-LPs at concentrations equivalent to 5 μg/ml Dox, and also the corresponding groups with verapamil (10 μM) respectively for 4 h incubation. To evaluate Dox internalization from different treatments, the corresponding cells were washed with ice-cold PBS and collected to measure intracellular Dox fluorescent intensity at 620 nm channel under flow cytometry (Beckman, FC 500).

2.6. Intracellular Dox retention of Dox-loaded liposomes

The intracellular retention of endocytosed liposomal Dox was observed under confocal microscope to investigate Dox efflux and retention in drug-resistant cells. Briefly, Bel7402 or Bel7402/5-FU cells were seeded on coverslips and pretreated with DMEM containing free Dox, Dox-PEG-LPs or Dox-TPGS-LPs at concentrations equivalent to 5 μg/ml Dox for 4 h (*i.e.*, time point 0 h for retention). Then the culture medium was changed and the cells were incubated with blank culture medium for another 4 h (*i.e.*, time point 4 h for retention). The cells were washed twice with ice-cold PBS and fixed with 4% paraformaldehyde solution for 30 min, followed by the staining of nuclei with DAPI (5 μg/ml) for 15 min, and then observed at 559 nm channel under confocal laser scanning microscope (CLSM, Olympus, FV1000).

Furthermore, the quantitative study was developed to calculate the Dox efflux rate by flow cytometry. Bel7402 or Bel7402/5-FU cells were attached to the bottom of 12-well plates to reach 5×10^5 cells per well, followed by treatment with DMEM containing various Dox formulations for 4 h at equivalent concentrations of 5 μg/ml Dox, respectively. Then the cells were washed twice with ice-cold PBS and further incubated with blank medium at 37 °C for 0–4 h. At predetermined time points, flow cytometry was adopted to measure the cell-associated Dox amount from the collected cells [32]. The intracellular retention efficiency (IRE) of Dox was deduced by the ratio of mean fluorescence intensities (MFI) of Dox at predetermined time points (*x* h) to MFI at 0 h of retention using the following formula:

$$IRE\ (\%) = \frac{MFI\ at\ x\ h\ of\ retention}{MFI\ at\ 0\ h\ of\ retention} \times 100\%$$

2.7. Intracellular distribution of siRNA/Dox-loaded liposomes

FAM-siRNA with green fluorescence was adopted instead of Bcl-2 siRNA to observe the intracellular siRNA distribution under confocal microscope (Olympus, FV1000). Bel7402/5-FU MDR cells were attached to the coverslips in 6-well plates to reach 8×10^5 cells per well. The cells were washed twice by using ice-cold PBS and then treated with culture medium containing FAM-siRNA/Dox-TPGS-LPs, FAM-siRNA/Dox-PEG-LPs, a mixture of free Dox and naked FAM-siRNA, and a mixture of free Dox and FAM-siRNA-TPGS-LPs for 4 h at 37 °C at equivalent concentrations of 5 μg/ml Dox and 100 nM FAM-siRNA. Subsequently, the cells were fixed and nuclei were stained with DAPI in accordance with the above described method. The channels of excitation wavelengths for DAPI, FAM-siRNA and Dox were 405 nm (blue), 488 nm (green) and 559 nm (red), respectively.

To quantitatively evaluate the intensive effect of siRNA on Dox internalization, the MFI of internalized Dox and FAM-siRNA in Bel7402/5-FU MDR cells after treating various liposomes were calculated by flow cytometry with the same protocol as described above. The detected channels of FAM-siRNA and Dox were 525 nm and 620 nm, respectively.

2.8. Western blot assay

Bel7402/5-FU MDR cells treated by various agents were incubated for 48 h, including DMEM, free Bcl-2 siRNA (100 nM), Bcl-2 siRNA/Dox-TPGS-LPs with low, middle, high Bcl-2 siRNA concentration at 25 nM, 50 nM and 100 nM. After the treatments, 2×10^6 cells were collected, washed and re-suspended in 50 μl ice-cold RIPA cell lysis buffer (containing 50 mM Tris–HCl, 150 mM NaCl, 1 mM EDTA, 1% Triton X-100, 1% sodium deoxycholate and 1% SDS; pH = 7.4) for 30 min, followed by centrifugation to collect the supernatant. Protein content was quantified by BCA assay. Sodium dodecyl sulfate–polyacrylamide gel electrophoresis (SDS-PAGE, 10%) was selected to differentiate proteins in each sample (20 μg/lane), followed by electrophoretical transfer to PVDF membranes (Millipore, USA). PBS containing 5% skim milk was used to block membranes that were then probed by the monoclonal antibody against Bcl-2 (1:1000, Santa Cruz, USA) and horse radish peroxidase (HRP) and goat anti-mouse antibody conjugate (1:3000, Santa Cruz, USA). Protein signals were visualized by chemiluminescence detection reagent (Boster, China) after the membranes were exposed to Kodak life science imaging films (Kodak, USA). The Bcl-2 potein expression level were normalized to the β-actin protein expression levels (internal standards).

2.9. Apoptosis assay

Bel7402/5-FU MDR cells were seeded and attached in 12-

well plates to reach 5×10^5 cells per well, followed by 48 h treatment with culture medium containing various formulations, including free Dox, Dox-PEG-LPs, Dox-TPGS-LPs, Bcl-2 siRNA-TPGS-LPs, Bcl-2 siRNA/Dox-PEG-LPs and Bcl-2 siRNA/Dox-TPGS-LPs, respectively. The concentrations of 0.5 μg/ml Dox and 100 nM Bcl-2 siRNA were selected for the test formulations. A control was maintained as untreated cells. The cells were subsequently collected, washed and re-suspended in 195 μl binding buffer, followed by the addition of 5 μl annexin V-FITC and 10 μl propidium iodide (PI). The mixture was gently blended by pipetting, and incubated for 15 min at room temperature. Flow cytometry was used to determine the proportions of apoptotic or stained cells [33].

2.10. Cytotoxicity

MTT assay was adopted to measure the *in vitro* cytotoxicity of various Dox-loaded liposomes in both Bel7402 and Bel7402/5-FU MDR cells [34]. Briefly, the cells were seeded in a 96-well plate (8×10^3 cells per well) and attached for 24 h. The cells were subsequently treated by free Dox, Dox-PEG-LPs, Dox-TPGS-LPs, Bcl-2 siRNA/Dox-TPGS-LPs at a range of Dox concentrations (0.02–20 μg/ml) for 24 and 48 h, respectively. With addition of 20 ul MTT solution (5 mg/ml), the cells were incubated for additional 4 h and then the medium was replaced by DMSO (150 ul). The Dox absorbanace in each well was measured at 570 nm by using microplate (Multiskan GO, Thermo Scientific, USA). The aforementioned experiment was repeated three times to get average IC_{50} values calculated by GraphPadprism 6 software.

2.11. Animal and tumor model

Male Balb/c nude mice (18–22 g, 5–6 weeks old) were obtained from Beijing Vital River Laboratory Animal Technology Co., Ltd (Beijing, China). The drug-resistant Bel7402/5-FU xenograft models (HCC-MDR) were generated by subcutaneous injection of 1×10^7 Bel7402/5-FU cells in 200 μl DMEM medium into the right flank of male BALB/c nude mice. The models were ready for experiments when the tumor grew to 100 mm^3. The animal studies were developed in compliance with the guideline on the care and use of laboratory animals of Huazhong University of Science and Technology. The guideline was authorized by the Animal Care Committee of Hubei Province, China (Approval Number: TY20120158).

2.12. The MDR tumor inhibitory rate in mice

The HCC-MDR mice with tumor inoculated were randomly separated into six groups ($n = 5$). Then, the mice in six groups were intravenously injected *via* the tail vein with normal saline, free Dox, Dox-PEG-LPs, Dox-TPGS-LPs, Bcl-2 siRNA/Dox-PEG-LPs and Bcl-2 siRNA/Dox-TPGS-LPs, respectively. The Dox and siRNA doses for the above formulations were 2 mg/kg and 0.6 mg/kg respectively every 3 d and total six doses. The time for the first dose administration was designated as Day 0. The tumor length and width were measured and the tumor volume was calculated by the following formula: $V = (L \times W^2)/2$, where L and W represent the length and width of the tumor. The tumor inhibitory rate (TIR) after 21 d treatment was introduced to compare tumor inhibition capacity among different formulations. TIR was deduced by the following equation:

$$\text{TIR}\ (\%) = \left(1 - \frac{\text{mean tumor volume of experimental group}}{\text{mean tumor volume of control group}}\right) \times 100\%$$

At the 21st d, all the mice were sacrificed. The tumor and major organs including heart, liver, spleen, lung, and kidney were collected, weighted and photographed. The collected organs and tissues were analyzed by hematoxylin–eosin (H&E) staining and immunnohistochemical staining of the terminal transferase dUTP nick-end labeling (TUNEL) assay to evaluate cell apoptosis in tumor. Western blot measured Bcl-2 protein expression level in tumor.

2.13. Statistical analysis

Results were shown as mean ± standard deviation (SD). One-way analysis of variance ANOVA was adopted to test statistical significance, which was set at $^*P < 0.05$, ** $P < 0.01$ or *** $P < 0.001$.

3. Results and discussion

3.1. The nanostructure and property of siRNA/Dox-TPGS-LPs

Dox-loaded cationic liposomes were prepared by the classical transmembrane ammonium sulfate gradient method with drug loading efficiency at around 8.7%. Bcl-2 siRNA was adsorbed to the surface of cationic liposomes Dox-TPGS-LPs or Dox-PEG-LPs *via* static electricity which resulted in the formation of Bcl-2 siRNA corona, namely Bcl-2 siRNA/Dox-TPGS-LPs or Bcl-2 siRNA/Dox-PEG-LPs. This nanostructure is enlightened by the biomimetic approach using plasma membrane or human serum albumin to modify the particle surface properties for the improved efficacy of nanosystems [35–37]. PEG-coated liposomes were selected as a control since PEG-DSPE was widely used in liposomes and showed good effect on *in vivo* anti-tumor drug delivery.

When the N:P ratio changed from 0.5:1 to 8:1, the particle size, zeta potential and entrapment efficiency of siRNA from Bcl-2 siRNA/Dox-TPGS-LPs were examined (Fig. S1). Zeta potential and entrapment efficiency of siRNA were increased accompanying with the increased N/P ratio, while the particle size change was irregular between 190–370 nm. The optimal N/P ratio is 4:1 with above 90% entrapment efficiency of siRNA.

The final characterization of the prepared liposomes are summarized in Table 1. The entrapment efficiency of Dox across all the prepared cationic liposomes was greater than 95%. Dox-PEG-LPs and Dox-TPGS-LPs had the similar diameter of approximately 130 nm, and their particle sizes increased to approximately 180–190 nm after loading with Bcl-2 siRNA. TEM observation (Fig. 2) showed that Dox-TPGS-LPs appeared uniform spherical shape, while Bcl-2 siRNA/Dox-TPGS-LPs

Table 1 – Characteristics of Dox-loaded cationic liposomes.

Formulations	Particle size (nm)	Polydispersity index	Zeta potential (mV)	Entrapment efficiency of Dox (%)
Dox-PEG-LPs	134.1 ± 0.6	0.031	17.5 ± 2.9	95.9 ± 1.8
Dox-TPGS-LPs	132.8 ± 1.1	0.053	32.7 ± 2.4	95.2 ± 2.1
Bcl-2 siRNA/Dox-PEG-LPs	178.0 ± 2.3	0.109	7.2 ± 1.8	95.6 ± 2.3
Bcl-2 siRNA/Dox-TPGS-LPs	192.4 ± 2.8	0.179	12.7 ± 2.1	95.1 ± 1.9

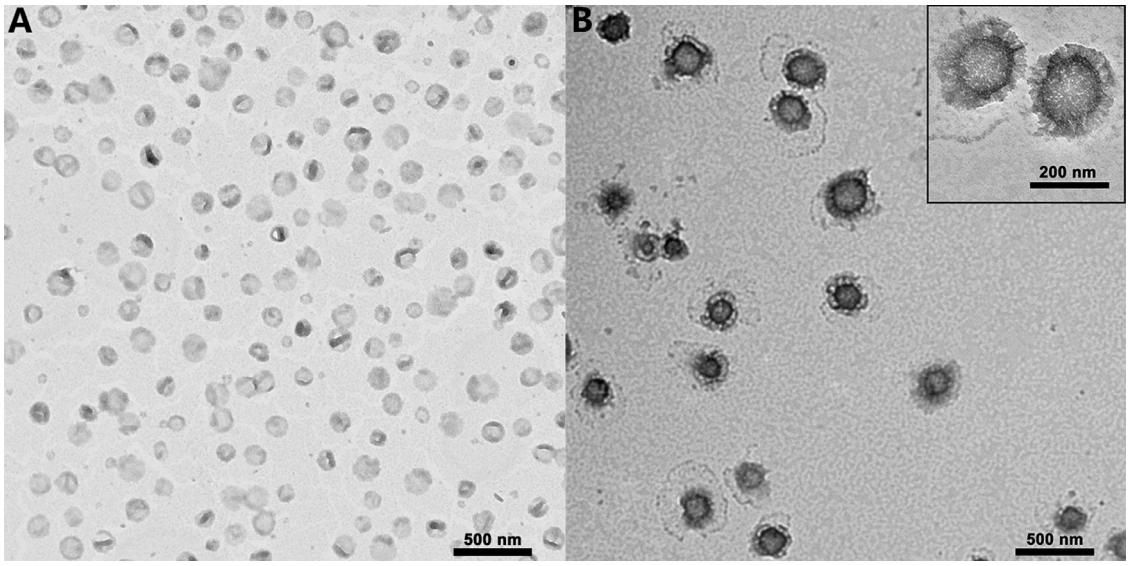

Fig. 2 – The nanostructure of Dox-TPGS-LPs (A) and Bcl-2 siRNA/Dox-TPGS-LPs (B) under TEM.

was observed with an additional corona layer on the liposome surface, indicating the successful loading of Bcl-2 siRNA on the surface of Dox-TPGS-LPs.

All the tested liposomes showed positive surface charge. Compared to the widely used PEG-modified liposomes, TPGS maintained the high zeta potential of cationic liposomes in favor of the electrostatic adsorption of siRNA-corona. As expected, the negatively charged Bcl-2 siRNA partly neutralized the positive charge of cationic liposomes, which led to decreased zeta potential of liposomes after loading with Bcl-2 siRNA.

The stability evaluation was shown in Fig. S3. After the presence of FBS in PBS, the particle sizes of Dox-PEG-LPs and Dox-TPGS-LPs increased by 10%–20% at 0 h, while those of Bcl-2 siRNA loaded liposomes showed no change with or without FBS. It indicated siRNA-corona could protect the liposomal core to avoid the attachment of FBS, probably due to the decreased surface positive potential causing a weak adsorption of nonspecific protein in blood circulation. The particle sizes of four liposomes containing siRNA or not in PBS with 10% FBS slowly climbed by ~20% until 96 h.

The hemolysis results (Fig. S4) showed good biocompatibility with 12%–15% hemolysis of Dox-PEG-LPs and Dox-TPGS-LPs for their relatively high positive surface charge, 7%–9% hemolysis of Bcl-2 siRNA/Dox-PEG-LPs and Bcl-2 siRNA/Dox-TPGS-LPs since the siRNA-corona decreased their surface charge.

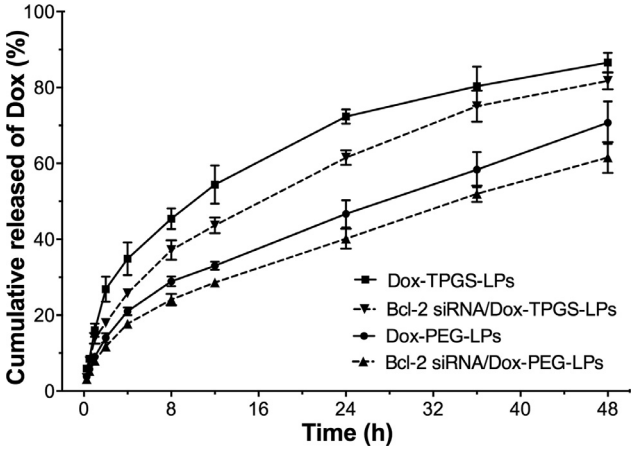

Fig. 3 – Dox release from various liposomes at 37 °C until 48 h. The medium is Tween 80 (1%, w/v)-containing PBS (0.01 M, pH 7.4). Data were expressed as mean ± SD ($n = 3$).

3.2. *Dox release from liposomes*

In vitro Dox release profile from Dox-PEG-LPs, Dox-TPGS-LPs, Bcl-2 siRNA/Dox-PEG-LPs and Bcl-2 siRNA/Dox-TPGS-LPs showed a sustained release up to 48 h (Fig. 3). Dox-TPGS-LPs exhibited a faster drug release than Dox-PEG-LPs, which probably could be due to the hydrophilic and solubilized

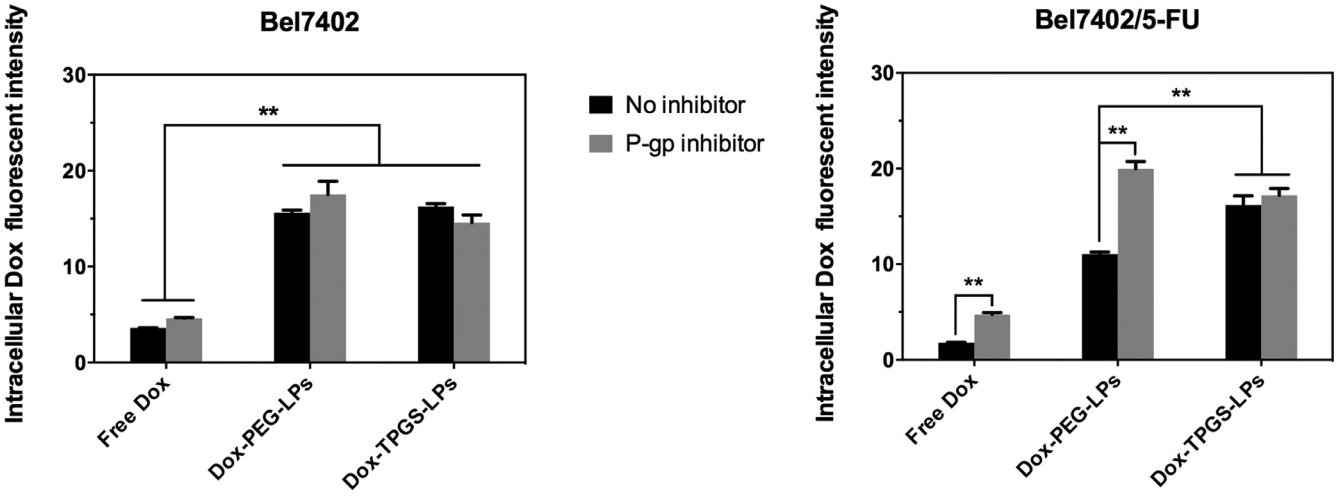

Fig. 4 – Intracellular Dox fluorescent intensity after applying different Dox formulations with or without P-gp inhibitor (verapamil). Bel7402 cells or Bel7402/5-FU MDR cells were treated with equivalent Dox concentration of 5 μg/ml for 4 h at 37 °C and then measured under flow cytometry. Data were expressed as mean ± SD ($n = 3$). **$P < 0.01$.

property of TPGS [38]. A relatively slow Dox release profile was observed in Bcl-2 siRNA/Dox-TPGS-LPs (*vs.* Dox-TPGS-LPs) and Bcl-2 siRNA/Dox-PEG-LPs (*vs.* Dox-PEG-LPs) which may be attributed to the siRNA-corona on the outside layer of Dox-loaded liposomes [27]. There's no significant difference of Dox release from Dox-TPGS-LPs and Bcl-2 siRNA/Dox-TPGS-LPs at 48 h (> 80%).

3.3. *Quantitative measurement of P-gp level in sensitive or MDR cells*

Immunofluorescence labeling experiments using flow cytometry were performed to quantify cellular P-gp expression levels in order to confirm upregulation of P-gp in Bel7402/5-FU MDR cells relative to Bel7402 cells. The result showed 1.23% and 44.8% of P-gp positive cells in Bel7402 and Bel7402/5-FU cells respectively (Fig. S2), which supported P-gp upregulation in multidrug resistant Bel7402/5-FU cells [39].

3.4. *TPGS inhibited P-gp efflux and improved Dox internalization*

To quantitatively compare the cellular internalization of the various formulations, Fig. 4 displays the Dox cellular internalization in Bel7402 cells and Bel7402/5-FU MDR cells.

In Bel7402 cells, cellular uptake of free Dox was lower than these in Dox-loaded liposomes groups, supporting that liposomes enhanced cellular uptake of enwrapped Dox. Dox-TPGS-LPs and Dox-PEG-LPs liposomes groups showed similar Dox uptake. In all treatment groups, the P-gp inhibitor verapamil had no significant impact on Dox uptake because of the low P-gp level in Bel7402 cells.

In Bel7402/5-FU MDR cells, cellular uptake of free Dox was lower than that observed in Bel7402 cells because of Dox efflux mediated by P-gp in Bel7402/5-FU MDR cells. Treatment with verapamil in Bel7402/5-FU MDR cells enhanced free Dox uptake to the level comparable to that observed in Bel7402 cells. Both Dox-TPGS-LPs and Dox-PEG-LPs liposomes enhanced cellular uptake of Dox with greater improvement observed in Dox-TPGS-LPs. Verapamil effectively enhanced intracellular Dox uptake in Dox-PEG-LPs group but not in Dox-TPGS-LPs groups. These results overall demonstrated that TPGS had similar effect as verapamil to inhibit P-gp and increase Dox internalization in drug-resistant Bel7402/5-FU cells.

3.5. *TPGS prolonged Dox retention time in drug-resistant cells*

The confocal image results in Fig. 5 showed the intracellular retention of Dox from different liposomes at 0 h and 4 h. The red Dox fluorescent intensity (FI) at 0 h and 4 h was similar between Dox-PEG-LPs and Dox-TPGS-LPs treatment groups in Bel7402 cells (Fig. 5A). On the other hand, in Bel7402/5-FU MDR cells, the red Dox FI in Dox-TPGS-LPs group was greater than that in Dox-PEG-LPs group at 0 h and 4 h, respectively, demonstrating that TPGS inhibited the exocytosis by P-gp and therefore improved Dox internalization amount and retention time in resistant cells.

The efflux rates of intracellular Dox and the intracellular retention curve of Dox by flow cytometry in Bel7402 and Bel7402/5-FU MDR cells for Dox-TPGS-LPs, Dox-PEG-LPs and free Dox are depicted in Fig. 6. In Bel7402 cells, Dox-TPGS-LPs and Dox-PEG-LPs demonstrated similar IRE-time courses with 75% of Dox retained by 4 h. By contrast, in Bel7402/5-FU MDR cells, Dox-TPGS-LPs exhibited a significantly high IRE-time course with 80% of Dox retained by 4 h, while 47% and 24% of Dox were retained for Dox-PEG-LPs and free Dox correspondingly. This indicated that TPGS strongly inhibited Dox exocytosis in drug-resistant cells and prolonged drug retention in Bel7402/FU cells.

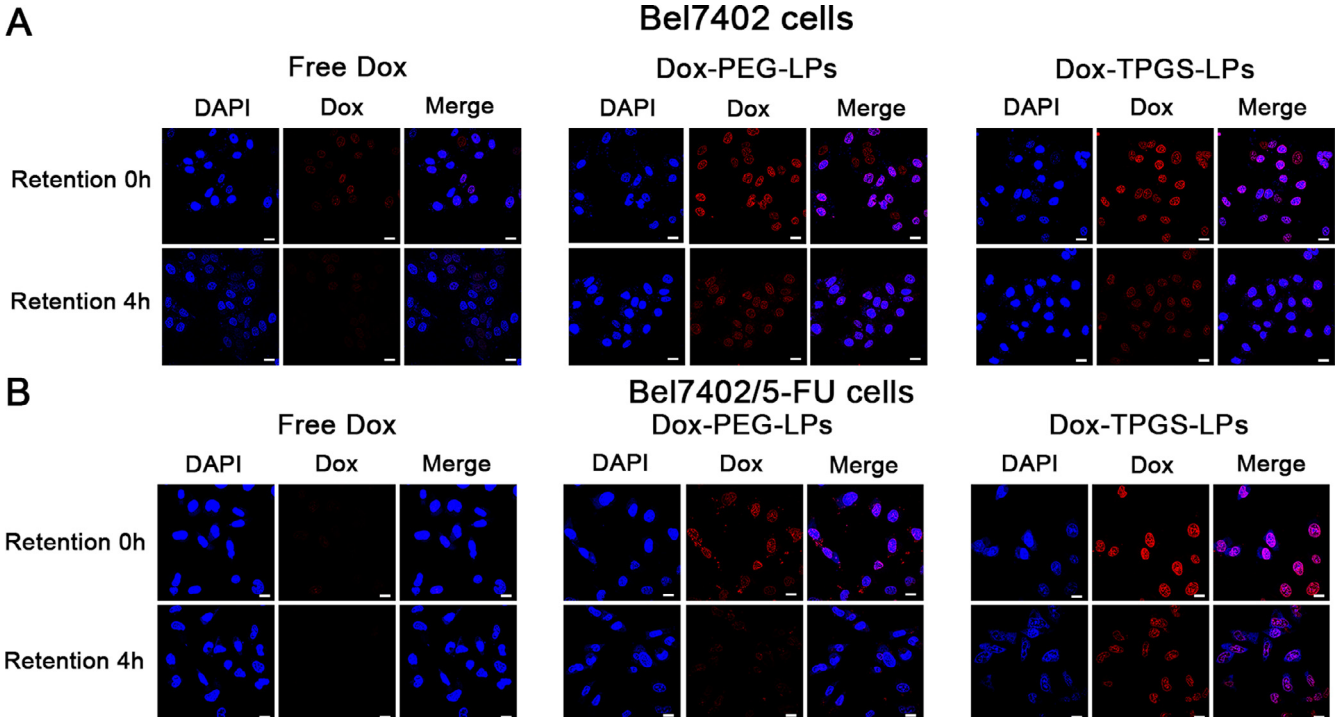

Fig. 5 – Confocal microscopic results of intracellular Dox retention in tumor cells. Bel7402 cells (A) and Bel7402/5-FU MDR cells (B) were pre-incubated with Dox-loaded formulations at 5 μg/ml for 4 h (*i.e.*, time point 0 h for retention), followed by incubation with fresh medium for another 4 h (*i.e.*, time point 4 h for retention). Bar: 20 μm.

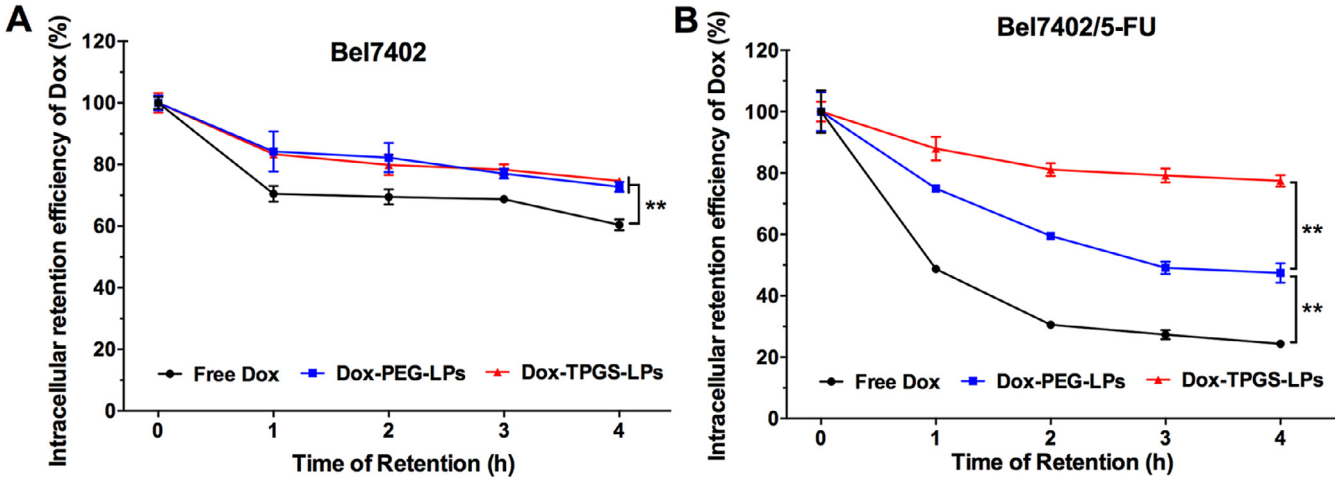

Fig. 6 – Intracellular Dox retention curves for 0–4 h with incubation of free culture medium in cells. Bel7402 (A) and Bel7402/5-FU (B) cells were pre-treated with free Dox, Dox-PEG-LPs, and Dox-TPGS-LPs containing 5 μg/ml of Dox for 4 h, respectively. Data were expressed as mean ± SD ($n = 3$). **$P < 0.01$.

3.6. *siRNA increased Dox internalization in drug-resistant cells by liposomes containing Dox and siRNA-corona*

To explore the effect of siRNA-corona on Dox delivery in Bel7402/5-FU MDR cells, intracellular distribution of endocytosed liposomes carrying FAM-siRNA and Dox were evaluated by confocal microscopy, as shown in Fig. 7A. Dox (red fluorescence) was transferred into nuclei and FAM-siRNA (green fluorescence) was scattered in the cytosol. In Bel7402/5-FU cells, FAM-siRNA/Dox-TPGS-LPs group demonstrated the strongest red Dox fluorescence compared with the other groups, while the green fluorescence of FAM-siRNA was similar between various FAM-siRNA loaded liposomes, no matter Dox was free or co-loaded in liposomes. Obviously, without the aid of liposomes, free Dox and naked FAM-siRNA seldom entered the Bel7402/5-FU MDR cells owing to the low efficiency of passive transport and the strong effect of drug

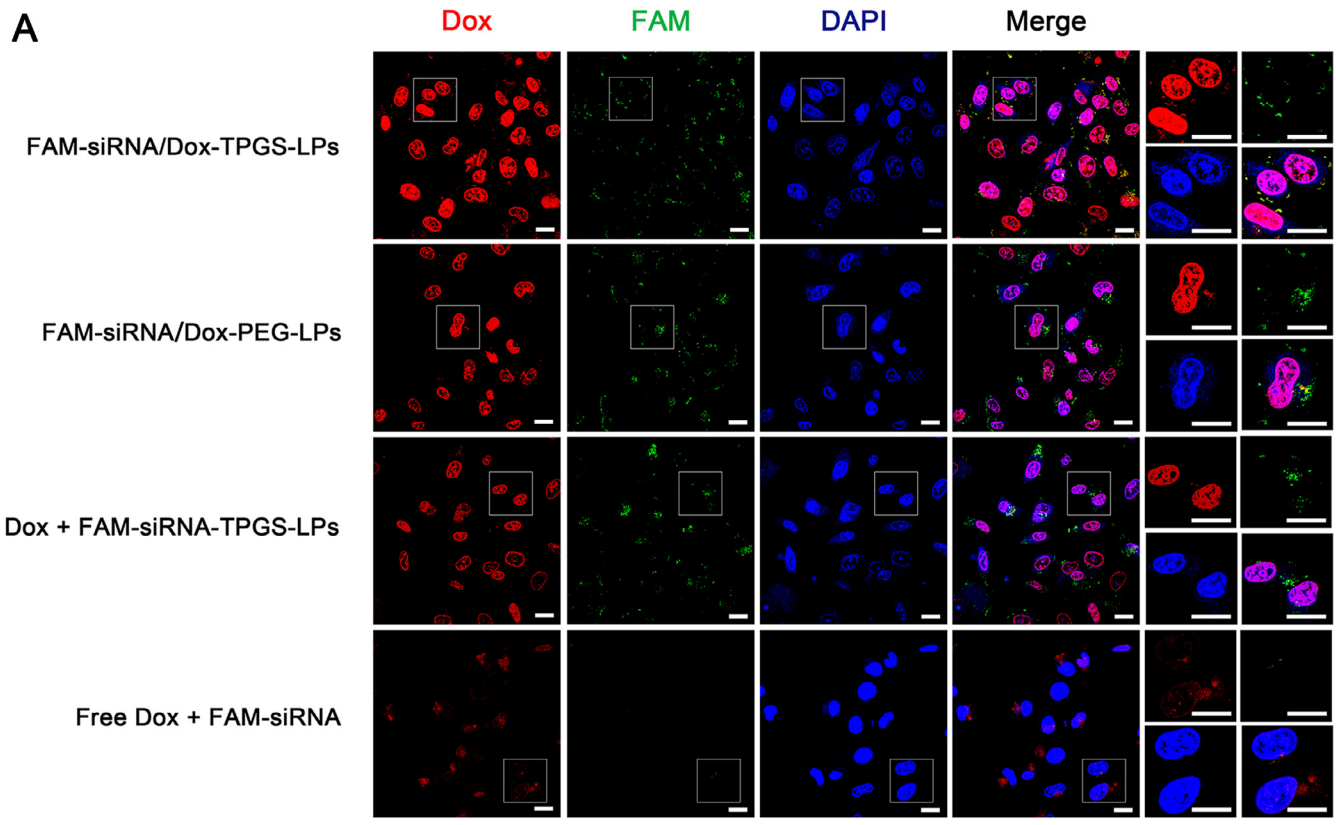

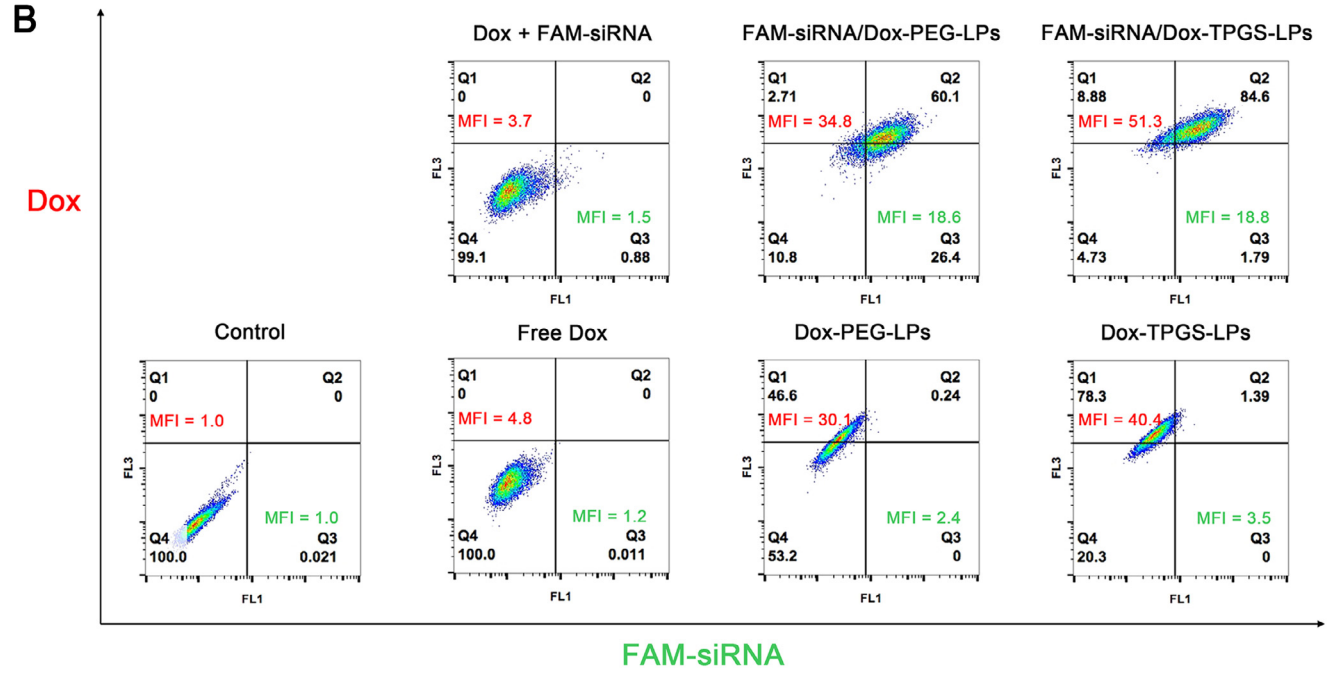

Fig. 7 – (A) Intracellular distribution of liposomes carrying Dox and FAM-siRNA in Bel7402/5-FU MDR cells evaluated by confocal microscope. The cells were incubated with FAM-siRNA/Dox-TPGS-LPs, FAM-siRNA/Dox-PEG-LPs, a mixture of free Dox and FAM-siRNA-TPGS-LPs and a mixture of free Dox and naked FAM-siRNA at 37 °C for 4 h. The red, green and blue colors stand for Dox, FAM-siRNA, and cell nucleus, respectively. The cells in the white box were magnified in the right column. Bar: 20 μm. (B) Quantitative analysis results of intracellular Dox and FAM-siRNA mean fluorescence intensities (MFI) from various formulations at 37 °C for 4 h in Bel7402/5-FU MDR cells by flow cytometry. The control group was treated with blank culture medium and the measured MFI was defined as "1". The equivalent initial concentrations of Dox and FAM-siRNA were 5 μg/ml and 100 nM, respectively.

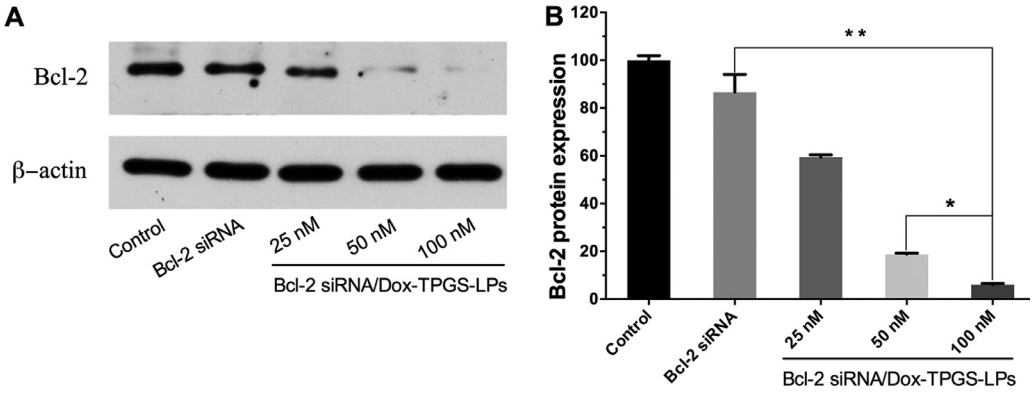

Fig. 8 – The Bcl-2 protein expression in Bel7402/5-FU MDR cells by western blot. (A) The cells were treated with naked Bcl-2 siRNA (100 nM) and Bcl-2 siRNA/Dox-TPGS-LPs at Bcl-2 siRNA concentration of 25, 50 and 100 nM for 48 h, respectively. The control group was treated with blank culture medium. β-actin was selected as the internal control. (B) The visualized protein signals were transferred to quantitative expression by ImageJ software. Data were expressed as mean ± SD ($n = 3$). *$P < 0.05$, **$P < 0.01$, compared with Bcl-2 siRNA/Dox-TPGS-LPs group (100 nM).

Table 2 – The priming effect of FAM-siRNA corona on the improvement of Dox uptake in Bel7402/5-FU cells.

MFI±SD	(1) PEG group	(2) TPGS group	$MFI_{(2)}/MFI_{(1)}$
(a) add siRNA#	34.8 ± 0.3	51.3 ± 1.8	1.47**
(b) only Dox	30.1 ± 0.6	40.4 ± 0.7	1.34**
$MFI_{(a)}/MFI_{(b)}$	1.16*	1.27**	

(1)(a) FAM-siRNA/Dox-PEG-LPs; (1)(b) Dox-PEG-LPs;.
(2)(a) FAM-siRNA/Dox-TPGS-LPs; (2)(b) Dox-TPGS-LPs.
MFI: mean fluorescence intensity of intracellular Dox.
*$P < 0.05$. ** $P < 0.05$.

efflux by P-gp. Interestingly, FAM-siRNA-TPGS-LPs improved free Dox internalization. These results suggested that FAM-siRNA-TPGS-LPs improved Dox internalization regardless whether Dox was co-loaded in liposomes or not.

To quantify the magnitude of the enhancement of Dox internalization by FAM-siRNA/Dox-TPGS-LPs, intracellular Dox and FAM-siRNA MFI in ten thousand cells from various Dox formulations were measured by flow cytometry (Fig. 7B). The MFI of control group treated with blank culture medium was defined as "1". Clearly, the green MFI of FAM-siRNA was 18.6–18.8 between FAM-siRNA/Dox-PEG-LPs and FAM-siRNA/Dox-TPGS-LPs, while that of free FAM-siRNA was only 1.5. It indicated over 12-fold increase of siRNA in cells by siRNA-loaded liposomes and TPGS didn't change cellular uptake of FAM-siRNA from liposomes. However, liposomes with FAM-siRNA corona did improve the uptake of Dox from PEG-modified or TPGS-linked liposomes, probably due to the size-dependent uptake of siRNA-loaded cationic liposomes and priming effect by siRNA-corona [40,41]. The quantitative improvement data were calculated in Table 2. The intracellular Dox MFI improvement by FAM-siRNA corona was 1.27- and 1.16-fold in TPGS group and in PEG group, respectively. And also the intracellular Dox MFI improvement of TPGS- *vs* PEG-modified liposomes with FAM-siRNA corona (1.47) was higher than the MFI of corresponding liposomes containing only Dox (1.34). These results proved the chemosensitizing effects of TPGS and siRNA-corona. FAM-siRNA/Dox-TPGS-LPs was superior to Dox-TPGS-LPs and FAM-siRNA/Dox-PEG-LPs in the improvement of Dox endocytosis in Bel7402/5-FU MDR cells.

3.7. *Bcl-2 siRNA/Dox-TPGS-LPs down-regulated Bcl-2 protein expression in Bel7402/5-FU MDR cells*

Bcl-2 protein has been shown as an anti-apoptosis factor influencing multiple drug resistance of malignant cells and treatment with chemotherapeutic agent such as doxorubicin or epirubicin could upregulate Bcl-2 protein level [42–44]. Western blot experiment evaluated Bcl-2 gene silencing effect by Bcl-2 siRNA in Bel7402/5-FU MDR cells (Fig. 8). Bcl-2 siRNA/Dox-TPGS-LPs (100 nM) significantly lowered the expression of Bcl-2 protein, while equivalent naked Bcl-2 siRNA cannot. It demonstrated the ability of Bcl-2 siRNA/Dox-TPGS-LPs to enter the cytosol. The decreased Bcl-2 protein level by Bcl-2 siRNA/Dox-TPGS-LPs showed a concentration-dependent silencing efficiency of 41%, 81% and 94%, respectively. 100 nM of Bcl-2 siRNA was selected in the current study to combine with Dox in TPGS-modified liposomes.

3.8. *Synergistic effects of Bcl-2 siRNA/Dox-TPGS-LPs on Bel7402/5-FU MDR cell apoptosis*

Fig. 9 illustrated the synergistic effect of TPGS, siRNA, and Dox delivered by Bcl-2 siRNA/Dox-TPGS-LPs on MDR tumor cell apoptosis. The four quadrants represented normal (Q4), early apoptotic (Q3), late apoptotic (Q2) and necrotic cells (Q1), respectively. The percentages of apoptotic cells were calculated from Q2 and Q3. Compared with other formulations, the Bcl-2 siRNA/Dox-TPGS-LPs group induced about 70% cell apoptosis. This apoptotic level is significantly higher than those in the Dox-TPGS-LPs group (47%), Bcl-2 siRNA/Dox-PEG-LPs group (30%), Dox-PEG-LPs group (21%), free Dox and Bcl-2 siRNA group (16%), free Dox group (14%). Obviously, TPGS-modified liposomes exhibited higher

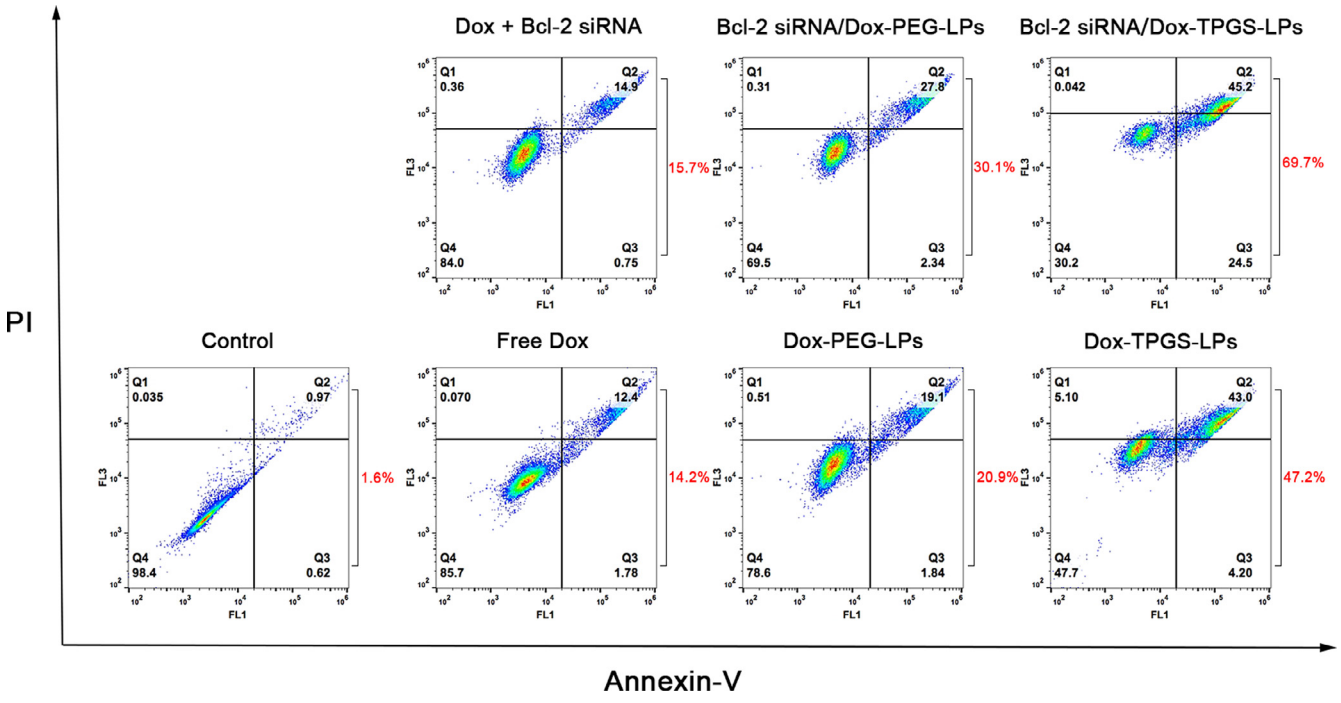

Fig. 9 – Apoptosis assay results in Bel7402/5-FU MDR cells treated by various Dox formualtions for 48 h. The control group is the untreated cells. The concentrations of Dox and Bcl-2 siRNA used were 0.5 μg/ml and 100 nM, respectively.

induction of cell apoptosis than PEG-linked liposomes and free Dox group, due to the enhanced Dox internalization by TPGS inhibiting P-gp efflux. To enhance apoptotic level, co-delivery of Dox and Bcl-2 siRNA was superior to mono-delivery of Dox. The cell apoptosis of Bcl-2 siRNA/Dox-TPGS-LPs group enhanced 23% compared to Dox-TPGS-LPs group, while that of Bcl-2 siRNA/Dox-PEG-LPs group had a slight enhancement about 9% compared to Dox-PEG-LPs. The combination of Dox, TPGS and Bcl-2 siRNA corona in cationic liposome systems significantly enhanced the drug-resistant cell apoptosis, which cannot be reached by each component used alone or by co-delivery of two components.

3.9. *Synergistic cytotoxic effect of Bcl-2 siRNA/Dox-TPGS-LPs*

MTT assay was used to measure the cooperative cytotoxic action of Dox, TPGS and Bcl-2 siRNA corona in cationic liposomes. The Bel7402 and Bel7402/5-FU MDR cells viabilities after various treatments were demonstrated (Fig. 10), with the corresponding IC_{50} values summarized in Table 3. As expected, the Bel7402/5-FU MDR cells exhibited obvious Dox-resistant behaviors during treatment in comparison with sensitive Bel7402 cells. For example, the IC_{50} of free Dox in Bel7402/5-FU MDR cells was over 100 μg/ml after incubation for 24 h based on the massive efflux of Dox, while that in Bel7402 cells was 2.71 μg/ml. It's approximately 50-fold difference in resistant to Dox between MDR cells and sensitive cells.

Table 3 – IC_{50} values of four Dox formulations against Bel7402 and Bel7402/5-FU cells calculated from MTT assay.

Formulations	IC_{50} values (μg/ml)			
	Bel7402		Bel7402/5FU	
	24 h	48 h	24 h	48 h
Free Dox	2.71	0.45	>100	12.03
Dox-PEG-LPs	1.51	0.20	55.09	1.97
Dox-TPGS-LPs	1.01	0.15	16.10	0.64
Bcl-2 siRNA/Dox-TPGS-LPs	0.40	0.09	4.31	0.18

In Bel7402 cells, free Dox entered the cells by passive diffusion and accumulated in the nuclei, while Dox-loaded liposomes were internalized in the cytoplasm followed by Dox released into the nuclei. The cytotoxicity was similar in Dox-PEG-LPs and Dox-TPGS-LPs (Fig. 10A, $P > 0.05$), while Bcl-2 siRNA/Dox-TPGS-LPs significantly increased cytotoxicity with decreased IC_{50} value (Fig. 10A, $P < 0.05$). The above results demonstrated the synergistic effect of Bcl-2 siRNA and Dox instead of the cytotoxic chemosensitizing effect of TPGS under the experimental concentrations in Bel7402 cells.

In Bel7402/5-FU MDR cells, TPGS-modified liposomes showed greater cytotoxicity than free Dox and Dox-PEG-LPs (Fig. 10B, $P < 0.05$). It's due to the drug efflux P-gp pump overexpressed on the surface of Bel7402/5-FU

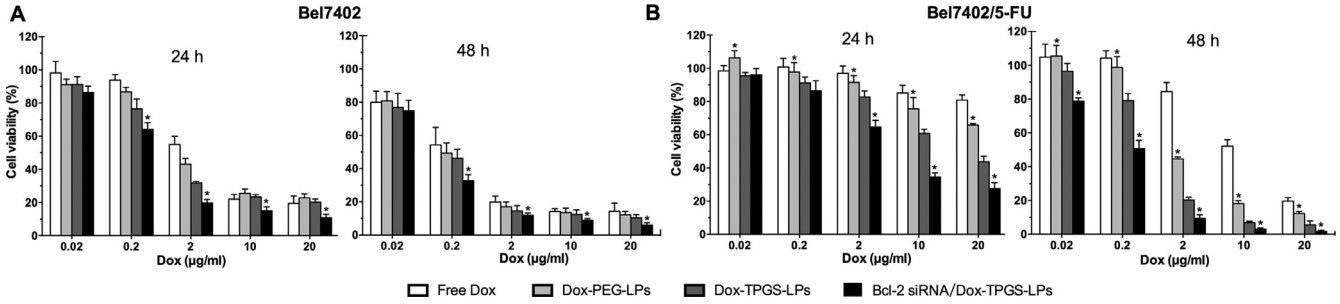

Fig. 10 – The cytotoxicity of various Dox formulations in Bel7402 (A) and Bel7402/5-FU (B) cells. The Dox concentration range: 0.02–20 μg/ml. Data were expressed as mean ± SD ($n = 3$). *$P < 0.05$, compared to Dox-TPGS-LPs group at equal concentrations of Dox.

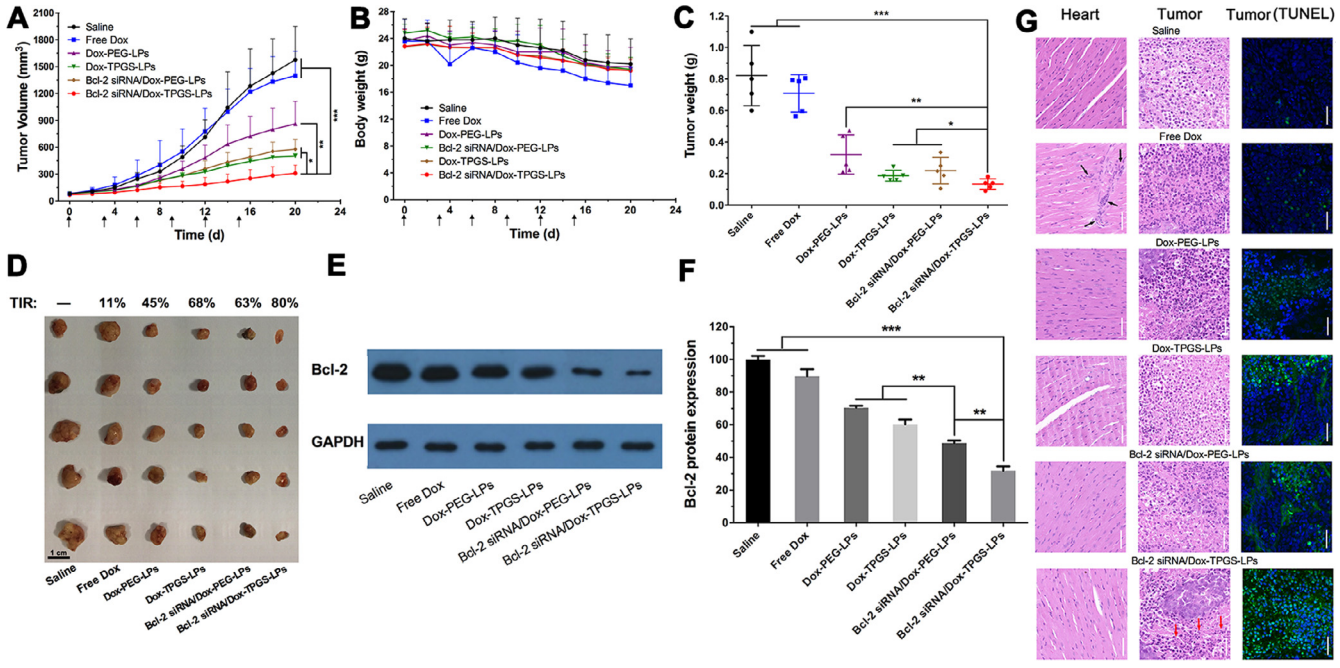

Fig. 11 – *In vivo* antitumor effect of various formulations in Bel7402/5-FU xenograft nude mice. Tumor volume (A) and body weight (B) changes. The arrows in *x* axis represent the time points of intravenous injection, *i.e.*, Day 0, 3, 6, 9, 12, 15. The intravenous injected single dose of Dox and siRNA was 2 mg/kg and 0.6 mg/kg, respectively ($n = 5$). Tumor weights (C) and images (D) at Day 21 from different treatment groups after the first administration. The tumor inhibitory rate (TIR) was deduced from the change of tumor volume. Black bar:1 cm. Bcl-2 expression level in tumors (E, F) and the H&E-staining of heart, tumor, TUNEL-staining of tumor slices (G) after 21 d treatment with various formulations. The black arrows indicate severe cardiotoxicity damage. The blue and green color stands for nucleus and apoptosis cell, respectively. GAPDH was adopted as the internal control. White scale bar: 50 μm. *$P < 0.05$, **$P < 0.01$, ***$P < 0.001$. (For interpretation of the references to colour in this figure legend, the reader is referred to the web version of this article.)

cells. Internalized Dox may be pumped, which resulted in reduced intracellular Dox concentration and led to MDR. TPGS may overcome the MDR. As a control, combined analysis from Dox internalization, retention and cytotoxicity results demonstrated no synergistic effect of TPGS in Bel7402 cells without increasing cellular accumulation of Dox. We further examined whether the inhibition of MDR dual-pathways was superior to inhibiting a single way. The IC_{50} value of Dox-TPGS-LPs was 3-fold lower than that of Dox-PEG-LPs, while that of Bcl-2 siRNA/Dox-TPGS-LPs approximated 4-fold lower than that of Dox-TPGS-LPs in Bel7402/5-FU cells. These results demonstrated the synergistic cytotoxic effects of TPGS-coated Dox liposomes with Bcl-2 siRNA corona on MDR cells.

3.10. *In vivo antitumor effect of Bcl-2 siRNA/Dox-TPGS-LPs in Bel7402/5-FU xenograft (HCC-MDR) nude mice*

The antitumor effect of Bcl-2 siRNA/Dox-TPGS-LPs was evaluated in drug-resistant Bel7402/5-FU xenograft tumor model in nude mice (Fig. 11). As discussed below, the *in vivo* tumor growth results overall supported the synergistic anti-

tumor efficacy of Dox, TPGS and Bcl-2 siRNA. It confirmed that the antitumor effect of chemotherapy may be greatly improved by simultaneously inhibiting drug efflux P-gp pump and anti-apoptotic chemoresistance Bcl-2 in Bel7402/5-FU xenograft nude mice.

We used saline as the control group because multiple liposomes formulations were used in this study and blank liposomes as vehicle control have been consistently reported to have no significant impact on tumor growth [27,45]. Free Dox did not inhibit tumor growth, showing similar results to the saline group (Fig. 11A), although the body weight has decreased for approximately 30% due to toxicity of Dox at the studied dose (Fig. 11B). This result has confirmed drug-resistant nature of the established HCC-MDR tumor model because minimal antitumor efficacy was achieved at the Dox dose that had resulted in severe side effect. The body weight was reduced by 18% in other Dox groups, suggesting PEG- or TPGS-linked liposomes improved tumor selectivity of drug effect and decreased the toxicity of Dox in normal organs. Note that the body weight in the saline group also decreased by approximately 15% probably due to the tumor burden and presence of tumor cachexia [46,47]. The tumor growth suppression of test liposome groups was 4–7 times that of free Dox group. Treatment with TPGS-modified liposomes resulted in slower tumor growth rate and smaller tumor size than PEG-linked liposomes. Fig. 11C demonstrated the greatest inhibiting effect on tumor growth reflected by smallest tumor size and lowest tumor weight. The TIR for Bcl-2 siRNA/Dox-TPGS-LPs was 80%, in comparison to 68% for Dox-TPGS-LPs and 63% for Bcl-2 siRNA/Dox-PEG-LPs (Fig. 11D). The TIR calculation from HCC-MDR nude mice showed the tumor growth suppression of Bcl-2 siRNA/Dox-TPGS-LPs group was 7 times that of free Dox group, and was superior to TPGS- or Bcl-2 siRNA- modified Dox liposomes. The results suggested the necessity and feasibility of dual suppression of drug resistance.

On Day 21, H&E staining results showed significant differences in the histological morphology of tumors receiving Bcl-2 siRNA/Dox-TPGS-LPs compared with other groups (Fig. 11G). Compared to other groups, a larger area of cell shrinkage, nuclear fragmentation in tumor cells and associated an increase in the TUNEL positive cell number were observed in the tumor cells treated by Bcl-2 siRNA/Dox-TPGS-LPs. The H&E staining pictures of heart showed cardiotoxicity damage in animals receiving free Dox group, which was not observed in animal treated with Bcl-2 siRNA/Dox-TPGS-LPs (Fig. 11G, black arrows). There was no significant difference in H&E staining results in other tissues across the various formulations (Fig. S5). The analysis of blood biochemical indicators (*i.e.,* heart-related LDH and CK-MB, liver-related ALT and AST, kidney-related BUN and CRE) showed the tested liposomes including Bcl-2 siRNA/Dox-TPGS-LPs didn't interfere the normal functions, while free Dox significantly decreased the expression of LDH and AST (Fig. S6).

As shown in Fig. 11E-11F, the cell apoptosis portion increased by 17% in tumor treated with Bcl-2 siRNA/Dox-TPGS-LPs than that with Bcl-2 siRNA/Dox-PEG-LPs ($P < 0.01$). The Bcl-2 protein expression ranged 60%−90% in the tumor treated by other Dox formulations. The significant difference of Bcl-2 protein expression between Bcl-2 siRNA/Dox-TPGS-LPs and TPGS- (or Bcl-2 siRNA-) modified Dox liposomes confirmed that Bcl-2 siRNA/Dox-TPGS-LPs effectively transferred to the cytosol of HCC-MDR tumor cells and maintained siRNA transfection functionality to down-regulate Bcl-2 protein level *in vivo*.

4. Conclusions

TPGS-coated cationic liposomes with Bcl-2 siRNA corona were successfully developed for reversing cancer MDR and for co-delivery of Dox. The current study is to test whether the inhibition of MDR dual-pathways is necessary and feasible to overcome drug resistance. The upregulated Bcl-2 and P-gp led to the 20–50 fold higher IC_{50} value of Dox in Bel7402/5-FU MDR cells than in sensitive cells. The anticancer efficacy was greatly decreased in HCC Bel7402/5-FU model due to Dox resistance. TPGS inhibited P-gp efflux and enhanced intracellular Dox concentration. Bcl-2 siRNA-corona maintained siRNA transfection functionality *in vivo* to downregulate anti-apoptotic Bcl-2 protein and primed Dox internalization (1.27 times that of Dox-TPGS-LPs). This multifunctional nanostructure was further demonstrated with improved anticancer activities of Dox. The *in vitro* cell apoptosis and cytotoxicity and *in vivo* antitumor experiments overall in drug-resistant HCC Bel7402/5-FU have demonstrated improved anticancer effect of Dox with increased induction of apoptosis and 7-fold greater effect than free Dox in tumor growth inhibition. In conclusion, we have shown that TPGS-coated cationic liposomes with siRNA corona has the capacity to simultaneously inhibit MDR dual-pathways and subsequently improve the activity of the chemotherapeutic agent co-delivered to a level that cannot be achieved by inhibiting a MDR single way.

Conflicts of interest

The authors declare that they have no competing interests.

Acknowledgements

This work was financially supported by National Basic Research Program of China (973 Program, 2015CB931802), and Natural Science Foundation of China (31470968 and 81627901). The authors acknowledged the aid of the Analytical and Testing Center of the College of Life Science and Technology at Huazhong University of Science and Technology in the testing of TEM, confocal microscopy and flow cytometry analysis.

Supplementary materials

Supplementary material associated with this article can be found, in the online version, at doi:10.1016/j.ajps.2019.10.003.

REFERENCES

[1] Wu Q, Yang Z, Nie Y, Shi Y, Fan D. Multi-drug resistance in cancer chemotherapeutics: mechanisms and lab approaches. Cancer Lett 2014;347:159–66.
[2] Gao Z, Zhang L, Sun Y. Nanotechnology applied to overcome tumor drug resistance. J Control Release 2012;162:45–55.
[3] Al-Lazikani B, Banerji U, Workman P. Combinatorial drug therapy for cancer in the post-genomic era. Nat Biotech 2012;30:679–91.
[4] Gottesman MM. Mechanisms of cancer drug resistance. Ann Rev Med 2002;53:615–27.
[5] Li JM, Zhang W, Su H, Wang YY, Tan CP, Ji LN, et al. Reversal of multidrug resistance in MCF-7/Adr cells by codelivery of doxorubicin and BCL2 siRNA using a folic acid-conjugated polyethylenimine hydroxypropyl-beta-cyclodextrin nanocarrier. Int J Nanomed 2015;10:3147–62.
[6] Yang XZ, Du XJ, Liu Y, Zhu YH, Liu YZ, Li YP, et al. Rational design of polyion complex nanoparticles to overcome cisplatin resistance in cancer therapy. Adv Mater 2014;26:931–6.
[7] Xing Y, Zhang J, Chen F, Liu J, Cai K. Mesoporous polydopamine nanoparticles with co-delivery function for overcoming multidrug resistance via synergistic chemo-photothermal therapy. Nanoscale 2017;9:8781–90.
[8] Pakunlu RI, Wang Y, Tsao W, Pozharov V, Cook TJ, Minko T. Enhancement of the efficacy of chemotherapy for lung cancer by simultaneous suppression of multidrug resistance and antiapoptotic cellular defense: novel multicomponent delivery system. Cancer Res 2004;64:6214–24.
[9] Saad M, Garbuzenko OB, Minko T. Co-delivery of siRNA and an anticancer drug for treatment of multidrug-resistant cancer. Nanomedicine 2008;3:761–76.
[10] Wu M, Liu X, Jin W, Li Y, Li Y, Hu Q, et al. Targeting ETS1 with RNAi-based supramolecular nanoassemblies for multidrug-resistant breast cancer therapy. J Control Release 2017;253:110–21.
[11] Wang AT, Liang DS, Liu YJ, Qi XR. Roles of ligand and TPGS of micelles in regulating internalization, penetration and accumulation against sensitive or resistant tumor and therapy for multidrug resistant tumors. Biomaterials 2015;53:160–72.
[12] Patil Y, Sadhukha T, Ma L, Panyam J. Nanoparticle-mediated simultaneous and targeted delivery of paclitaxel and tariquidar overcomes tumor drug resistance. J Controll Release 2009;136:21–9.
[13] Wang F, Zhang D, Zhang Q, Chen Y, Zheng D, Hao L, et al. Synergistic effect of folate-mediated targeting and verapamil-mediated P-gp inhibition with paclitaxel-polymer micelles to overcome multi-drug resistance. Biomaterials 2011;32:9444–56.
[14] Bao Y, Yin M, Hu X, Zhuang X, Sun Y, Guo Y, et al. A safe, simple and efficient doxorubicin prodrug hybrid micelle for overcoming tumor multidrug resistance and targeting delivery. J Control Release 2016;235:182–94.
[15] Guo Y, Luo J, Tan S, Otieno BO, Zhang Z. The applications of vitamin E TPGS in drug delivery. Eur J Pharm Sci 2013;49:175–86.
[16] Cheng D, Cao N, Chen J, Yu X, Shuai X. Multifunctional nanocarrier mediated codelivery of doxorubicin and siRNA for synergistic enhancement of glioma apoptosis in rat. Biomaterials 2012;33:1170–9.
[17] Yin T, Wang P, Li J, Wang Y, Zheng B, Zheng R, et al. Tumor-penetrating codelivery of siRNA and paclitaxel with ultrasound-responsive nanobubbles hetero-assembled from polymeric micelles and liposomes. Biomaterials 2014;35:5932–43.
[18] Huang HY, Niu JL, Lu YH. Multidrug resistance reversal effect of DMC derived from buds of cleistocalyx operculatus in human hepatocellular tumor xenograft model. J Sci Food Agric 2012;92:135–40.
[19] Maluccio M, Covey A. Recent progress in understanding, diagnosing, and treating hepatocellular carcinoma. CA Cancer J Clin 2012;62:394–9.
[20] Su Y, Wang K, Li Y, Song W, Xin Y, Zhao W, et al. Sorafenib-loaded polymeric micelles as passive targeting therapeutic agents for hepatocellular carcinoma therapy. Nanomedicine 2018;13:1009–23.
[21] Shi LX, Ma R, Lu R, Xu Q, Zhu ZF, Wang L, et al. Reversal effect of tyroservatide (YSV) tripeptide on multi-drug resistance in resistant human hepatocellular carcinoma cell line BEL-7402/5-FU. Cancer Lett 2008;269:101–10.
[22] Huang HY, Niu JL, Zhao LM, Lu YH. Reversal effect of 2′,4′-dihydroxy-6′-methoxy-3′,5′-dimethylchalcone on multi-drug resistance in resistant human hepatocellular carcinoma cell line BEL-7402/5-FU. Phytomedicine 2011;18:1086–92.
[23] Wei DD, Wang JS, Kong LY. Reversal effects of components from the fruits of illicium simonsii on human adriamycin-resistant MCF-7 and 5-Fluorouracil-resistant BEL7402 cells. Phytotherapy Res 2011;26:562–7.
[24] Zhao X, Chen Q, Li Y, Tang H, Liu W, Yang X. Doxorubicin and curcumin co-delivery by lipid nanoparticles for enhanced treatment of diethylnitrosamine-induced hepatocellular carcinoma in mice. Eur J Pharm Biopharm 2015;93:27–36.
[25] Barenholz Y. Doxil(R)–the first FDA-approved nano-drug: lessons learned. J Control Release 2012;160:117–34.
[26] Li Y, Gao L, Tan X, Li F, Zhao M, Peng S. Lipid rafts-mediated endocytosis and physiology-based cell membrane traffic models of doxorubicin liposomes. Biochim Biophys Acta 2016;1858:1801–11.
[27] Qu MH, Zeng RF, Fang S, Dai QS, Li HP, Long JT. Liposome-based co-delivery of siRNA and docetaxel for the synergistic treatment of lung cancer. Int J Pharm 2014;474:112–22.
[28] Zhang J, Du Z, Pan S, Shi M, Li J, Yang C, et al. Overcoming multidrug resistance by codelivery of MDR1-targeting siRNA and doxorubicin using EPHA10-mediated pH-sensitive lipoplexes: *in vitro* and *in vivo* evaluation. ACS Appl Mater Interfaces 2018;10:21590–600.
[29] Gao Y, Jia L, Wang Q, Hu H, Zhao X, Chen D, et al. pH/Redox dual-responsive polyplex with effective endosomal escape for codelivery of siRNA and doxorubicin against drug-resistant cancer cells. ACS Appl Mater Interfaces 2019;11:16296–310.
[30] Wang L. Preparation and *in vitro* evaluation of an acidic environment-responsive liposome for paclitaxel tumor targeting. Asian J Pharm Sci 2017;12:470–7.
[31] Liu X, Li Y, Tan X, Rao R, Ren Y, Liu L, et al. Multifunctional hybrid micelles with tunable active targeting and acid/phosphatase-stimulated drug release for enhanced tumor suppression. Biomaterials 2018;157:136–48.
[32] Ma YC, Wang JX, Tao W, Sun CY, Wang YC, Li DD, et al. Redox-responsive polyphosphoester-based micellar nanomedicines for overriding chemoresistance in breast cancer cells. ACS Appl Mater Interfaces 2015;7:26315–25.
[33] Wang Q, Zhang C, Shen G, Liu H, Fu H, Cui D. Fluorescent carbon dots as an efficient siRNA nanocarrier for its interference therapy in gastric cancer cells. J Nanobiotech 2014;12:58.
[34] Tang B, Fang G, Gao Y, Liu Y, Liu J, Zou M, et al. Lipid-albumin nanoassemblies co-loaded with borneol and paclitaxel for intracellular drug delivery to C6 glioma cells with P-gp inhibition and its tumor targeting. Asian J Pharm Sci 2015;10:363–71.

[35] Xuan M, Shao J, Dai L, Li J, He Q. Macrophage cell membrane camouflaged au nanoshells for *in vivo* prolonged circulation life and enhanced cancer photothermal therapy. ACS Appl Mater Interfaces 2016;8:9610–18.
[36] Cao H, Zou L, He B, Zeng L, Huang Y, Yu H, et al. Albumin biomimetic nanocorona improves tumor targeting and penetration for synergistic therapy of metastatic breast cancer. Adv Funct Mater 2017;27:1605679.
[37] Pei Q, Hu X, Zheng X, Liu S, Li Y, Jing X, et al. Light-activatable red blood cell membrane-camouflaged dimeric prodrug nanoparticles for synergistic photodynamic/chemotherapy. ACS Nano 2018;12:1630–41.
[38] Muthu MS, Kulkarni SA, Xiong J, Feng SS. Vitamin E TPGS coated liposomes enhanced cellular uptake and cytotoxicity of docetaxel in brain cancer cells. Int J Pharm 2011;421:332–40.
[39] Gottesman MM, Fojo T, Bates SE. Multidrug resistance in cancer: role of ATP-dependent transporters. Nat Rev Cancer 2002;2:48–58.
[40] Liang S, Yang XZ, Du XJ, Wang HX, Li HJ, Liu WW, et al. Song E-W: optimizing the size of micellar nanoparticles for efficient siRNA delivery. Adv Funct Mater 2015;25:4778–87.
[41] Wang J, Lu Z, Wang J, Cui M, Yeung BZ, Cole DJ, et al. Paclitaxel tumor priming promotes delivery and transfection of intravenous lipid-siRNA in pancreatic tumors. J Control Release 2015;216:103–10.
[42] Cao N, Cheng D, Zou S, Ai H, Gao J, Shuai X. The synergistic effect of hierarchical assemblies of siRNA and chemotherapeutic drugs co-delivered into hepatic cancer cells. Biomaterials 2011;32:2222–32.
[43] Chen W, Liu X, Xiao Y, Tang R. Overcoming multiple drug resistance by spatial-temporal synchronization of epirubicin and pooled siRNAs. Small 2015;11:1775–81.
[44] Kong L, Xing L, Zhou B, Du L, Shi X. Dendrimer-modified MoS_2 nanoflakes as a platform for combinational gene silencing and photothermal therapy of tumors. ACS Appl Mater Interfaces 2017;9:15995–6005.
[45] Zhang BF, Xing L, Qiao JB, Cui PF, Wang FZ, Zhang JL, et al. *In vivo* synergistic antitumor effect and safety of siRNA and lonidamine dual-loaded hierarchical targeted nanoparticles. Int J Pharm 2016;506:207–13.
[46] Kwak G, Jo SD, Kim D, Kim H, Kim MG, Kim K, et al. Synergistic antitumor effects of combination treatment with metronomic doxorubicin and VEGF-targeting RNAi nanoparticles. J Control Release 2017;267:203–13.
[47] Ye Z, Wu WR, Qin YF, Hu J, Liu C, Seeberger PH, et al. An integrated therapeutic delivery system for enhanced treatment of hepatocellular carcinoma. Adv Funct Mater 2018;28:1706600.